Model calculation of NMR satellite data for iron-group atoms in copper

J. David Cohen* and Charles P. Slichter
Department of Physics and Materials Research Laboratory, University of Illinois at Urbana-Champaign, Urbana, Illinois 61801
(Received 25 January 1980)

We report model calculations of NMR satellite data for iron-group impurity atoms in Cu which provide a tractable method for relating the experimentally observed Knight shifts to the structure of the magnetic atoms. This model is based on a three-parameter one-electron screened potential with exchange. For Fe, Mn, and Cr impurities we obtain the positions and widths of Anderson-like scattering resonances and find that the numbers of d electrons are nearly integral and indicate $3d^7$, $3d^5$, and $3d^4$ configurational assignments, respectively. The model gives good agreement with near-neighbor Knight shifts, is consistent with bulk susceptibility and high-temperature resistivity, and in most cases agrees with the axial component of the measured anisotropic Knight shifts. We also relate our results to NMR line-broadening data and near-neighbor quadrupole data. The model is formulated to include the case of impurities without a zero-field magnetic moment and is easily extended to account for trends observed as one moves across the entire iron group.

I. INTRODUCTION

Details of the electronic structure of $3d$ impurities in nonmagnetic host metals remain largely unresolved in spite of the great interest these systems have received in over a decade of active research. Experimental techniques such as ESR (electron spin resonance), ENDOR (electron nuclear double resonance), or optical-absorption measurements which have been so important in understanding properties of electronic structure of magnetic impurities in insulators have severe limitations or are very difficult to interpret when the host is a metal. However, NMR studies of the impurity atom[1,2] and of the spin density at the host near neighbors to these impurities[3,4] in measurements of the so-called "satellite" spectra have proven very powerful in studying details of impurity moment formation and of the moment-conduction electron coupling. At present, satellite measurements have been reported for all the iron-group atoms in copper.[5] Of particular importance are the recent studies of Mn, Cr, Fe, and Co impurities in single-crystal copper samples[6–8] which, through unambiguous assignment of satellite lines to specific neighbor shells, have provided an actual map of the spin density as a function of distance near these impurities.

Although it has been generally accepted that such measurements reflect details of the electronic structure of the impurities themselves, previous attempts to make this relationship quantitative have had only limited success. One way of formulating this relation is via scattering phase shifts such as in the Friedel-Anderson approach.[9,10] However, the well-known Ruderman-Kittel-Kasuya-Yosida (RKKY) form of the spin density, based on a point interaction between the conduction electrons and the impurity, is not adequate for describing the spin density at the near neighbors and consistently produces the wrong sign Knight shifts near the impurity. Jena and Geldart[11] have pointed out that the near-neighbor spin density is especially sensitive to scattering by conduction electrons significantly below the Fermi surface. For this reason calculations that are restricted to behavior at the Fermi energy, though adequate for interpreting many experimental properties of these systems (such as spin-relaxation rates, NMR line broadening, residual resistivity, de Haas-van Alphen damping, etc.), are unsuitable for describing the near-neighbor Knight shifts.

In order to be able to extract meaningful conclusions from a more detailed description of the interaction, any model must be sufficiently simple that it can be parametrized easily from the experimental data. This is the most serious drawback to the approach used by Jena and Geldart based on the Anderson model. While they offer an interpolation formula to circumvent this difficulty, this formula is valid over a very restricted range of its parameters and has not proved useful in practice.[12]

Our approach has been to develop a one-electron model, based on a screened atomiclike potential with exchange to represent the magnetic impurity, which we solve numerically for electrons throughout a spherical "host-metal" conduction band.[13] Although many properties of the magnetic atom require a more complete treatment in terms of a many-body theory, such a one-electron potential, assumed to represent an average of the many-body configurations of the

magnetic atom, is easily solved and, as we demonstrate, offers a reasonably complete description of the experimental data.

The one-electron potential is constructed to reflect the following facts: (i) Inside the core region of the impurity the electric field is very similar to that of the free atom apart from a small screening correction. (ii) Outside this region, screening leads to an essentially flat potential. (iii) Since the atom is magnetic we must employ a different potential for up and down spin. The transition between the regions described in (i) and (ii) is made simply by means of a step. In (iii) we have implicitly assumed we are dealing with a magnetic atom which is "spin-split" and so treat the two spin levels independently. This has been the approach taken in the early work of Friedel[9] as well as by Jena and Geldart,[11] and others.[14,15] Such an assumption is probably valid for the strongly magnetic systems of *Cu*Cr, *Cu*Mn, and *Cu*Fe. We develop an alternate formulation for systems, such as *Cu*Co, for which there may not be a well-formed moment.

Two problems which do require a multielectron description are the Kondo effect and the correct treatment of configurational degrees of freedom within the $3d$ impurity atom. The former has been shown experimentally to enter only as a factor of the impurity susceptibility and does not affect the spatial dependence of the magnetization at the near neighbors even at temperatures far below the Kondo temperature.[3,16] The configurational character of the impurity represents a more serious difficulty within the present model. It is discussed in Secs. IV C and VI.

We omit other known features of these systems. A crystal field seems to play a significant role experimentally in certain cases. We comment briefly on including a crystal potential in the model in Sec. V but generally omit such considerations. There are discrepancies which we attribute to the presence of the copper d bands. We nonetheless omit any details of the host band structure or Fermi surface. We have also ignored any role of spin-orbit coupling in our description of the magnetic atom, contrary to some recent experimental results. We shall return to a discussion of some of these points in the final section of this paper.

II. COMPUTATION OF SATELLITE SHIFTS

A general discussion of the origin and interpretation of the different "satellite" lines in copper containing $3d$ transition-metal impurities can be found in the single-crystal studies of Stakelon and Slichter[6] and Aton *et al.*[7] We will be mainly concerned with those shifts originating from the hyperfine coupling between the copper nuclear moment $\vec{\mu}_N$ and the spin of nearby electrons $\vec{S}_j$,

$$\mathcal{H}_{\rm hf}=\sum_j \tfrac{8}{3}\pi\gamma_e\hbar\,\vec{\mu}_N\cdot\vec{S}_j\delta(\vec{r}_j-\vec{R}_n)+\sum_j \gamma_e\hbar\,\vec{\mu}_N\cdot\left[\frac{3(\vec{r}_j-\vec{R}_n)[\vec{S}_j\cdot(\vec{r}_j-\vec{R}_n)]}{|\vec{r}_j-\vec{R}_n|^5}-\frac{\vec{S}_j}{|\vec{r}_j-\vec{R}_n|^3}\right], \tag{1}$$

where $\vec{R}_n$ and $\vec{r}_j$ denote the position vectors of the copper nucleus and electrons, respectively. The first term in Eq. (1) is the usual Fermi contact term which gives rise to the Knight shift in pure copper and is the dominant mechanism for producing the satellite shifts in most of the copper-$3d$ alloys. It produces the same shift for all copper nuclei in a given neighbor shell (independent of the orientation of applied field with respect to the crystal axes). The second term represents the dipolar interaction between nuclear and electron moments and gives rise to anisotropic shifts. Both forms of coupling have been observed in single-crystal copper samples containing Cr, Mn, Fe, and Co impurities. The anisotropic coupling will be treated in detail in Sec. V. In that section we will also comment on the electric quadrupole coupling observed in many of these alloys.

The interaction given in Eq. (1) can also be expressed as an effective field

$$\mathcal{H}_{\rm hf}=-\vec{\mu}_N\cdot\delta\vec{H}_{\rm eff}(\vec{R}_n) \tag{2}$$

caused by the polarization by an applied field $\vec{H}_0$ of the electron spins in a metal or, as is often more customary, in terms of a second rank tensor $\vec{K}$ (called the Knight-shift tensor)

$$\mathcal{H}_{\rm hf}=-\vec{\mu}_N\cdot\vec{K}(\vec{R}_n)\cdot\vec{H}_0\ . \tag{3}$$

We display the dependence on $\vec{R}_n$ explicitly since the field will vary with the relative position of the copper nucleus to the magnetic impurity.

We shall postpone treatment of the dipole coupling until Sec. V and outline in our present discussion the method for calculating the isotropic satellite splittings from the one-electron impurity potential to be described in Sec. III. Let us denote the electronic wave functions in the metal by $\Psi_{\alpha\sigma}(\vec{r})$ where we explicitly recognize that the spatial form of these wave functions may depend on the spin σ (α denotes the remaining quantum numbers). Then the contact term in Eq. (1) will contribute an effective field at the nth nucleus given by

$$\delta H(\vec{R}_n)=-\tfrac{8}{3}\pi\sum_{\alpha\sigma}|\Psi_{\alpha\sigma}(\vec{R}_n)|^2\gamma_e\hbar m_{\alpha\sigma}P_{\alpha\sigma}\ , \tag{4}$$

where $P_{\alpha\sigma}$ denotes the occupation of the state $\Psi_{\alpha\sigma}$. Since the observed satellite shifts are due to the *extra*

field caused by the presence of a nearby impurity we should subtract from $\delta H(\vec{R}_n)$ the Knight shift of the pure metal. This gives us

$$\delta H_l(\vec{R}_n)=\tfrac{8}{3}\pi\gamma_e\hbar\sigma(\vec{R}_n) \ ,$$

where

$$\sigma(\vec{R}_n)=-\sum_{\alpha\sigma}[|\Psi_{\alpha\sigma}(\vec{R}_n)|^2-|\Psi^0_{\alpha\sigma}(\vec{R}_n)|^2]m_{\alpha\sigma}P_{\alpha\sigma} \tag{5}$$

denotes the extra spin density surrounding the impurity. Thus the problem now becomes one of determining the wave functions $\Psi_{\alpha\sigma}(\vec{R}_n)$. ($\Psi^0_{\alpha\sigma}$ denotes the wave functions for the pure metal.)

Let us consider that the effect of the impurity on the host-metal bands is to give rise to a spherically symmetric one-electron potential. We shall further simplify the problem by ignoring the host band structure and assume free-electron bands. We can then express the solution outside the impurity region in the customary manner in terms of spherical functions and scattering phase shifts

$$\Psi_{kl\sigma}\sim[\cos\delta_{l\sigma}j_l(kr)-\sin\delta_{l\sigma}n_l(kr)]Y_{lm}(\Theta,\phi) \ ,$$
$$\Psi^0_{kl\sigma}\sim j_l(kr)Y_{lm}(\Theta,\phi) \ . \tag{6}$$

In general we must still properly orthogonalize these functions to the copper core states. This is absolutely essential for the calculation of the anisotropic shifts in Sec. V. For the Fermi contact term, however, orthogonalization results primarily in a constant enhancement factor which can be determined experimentally from the pure-metal Knight shift. In particular, expressing the satellite shifts as ratios to the Knight shift in the pure metal allows us to perform the calculation of the isotropic shifts using free-electron wave functions.

We now consider the application of a static magnetic field. It is necessary to distinguish between impurities with or without a permanent moment. For the latter case we simply set $P_{\alpha\sigma}$ in Eq. (5) equal to the Fermi function $f(E_{\alpha\sigma},T)$. For the spin-split case we must further label the impurity spin degrees of freedom since the scattering of a conduction electron

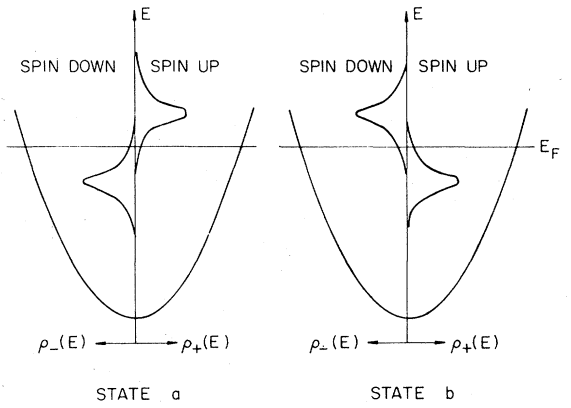

FIG. 1. Density of states in the Anderson model. This shows the densities for up- and down-spin electrons vs energy E contribution by the magnetic impurity. The parabolic curves of a free electron are also shown. State a corresponds to an impurity with a net spin down, hence net spin magnetic moment up. State b has a net down spin and up moment.

from an impurity with spin will depend on the orientation of its spin with respect to the applied field. Thus $P_{\alpha\sigma}$ becomes $P^c_{\alpha\sigma}=P_c f(E_{\alpha\sigma},T)$ where P_c gives the relative occupations of the different impurity moment orientations. We similarly label the electron wave functions. In our discussion below we shall simplify the problem by considering only two moment orientations, a and b, as in the original formulation of the Anderson Hamiltonian (see Fig. 1). The nonspin-split case may be treated within the same notation with a single value for c.

Application of a field H_0 will cause a net spin polarization even when there is no permanent moment due to (i) a difference of the Fermi function $f(E_{\alpha\sigma},T)$ for different σ and (ii) a perturbation of the scattering levels of the impurity. In the spin-split case, it also determines the population of the different moment orientations P_c. Incorporating the free-electron wave functions of Eq. (6) we explicitly display this field dependence of the hyperfine fields

$$\delta H_l(\vec{R}_n)=-\tfrac{8}{3}\pi\gamma_e\hbar\sum_{cl\sigma}\frac{(2l+1)}{\Omega}m_\sigma\int\rho_1(W_k)dW_k\{[n_l^2(kr)-j_l^2(kr)]\sin^2\delta f_\sigma(H_0)-2n_l(kr)j_l(kr)$$
$$\times\sin\delta f_\sigma(H_0)\cos\delta f_\sigma(H_0)\}P_c f(W_{k\sigma},T) \ , \tag{7}$$

where we have averaged over the angular functions and where $\rho_1(W_k)$ is the density of states of one spin for volume Ω. Since the spin dependence of the scattering is due to the unfilled d levels of the impurity, it is the d-wave scattering that will essentially determine δH_l. In the following discussion it suffices to keep only the d-wave contribution. We will now consider the two basic kinds of impurities in turn.

A. Spin-split case

The strongly magnetic systems of Cr, Mn, and Fe in copper are expected to belong to this class and are characterized by a Curie-Weiss temperature-dependent susceptibility. In this case the effect of the applied field on the levels is small (see Appendix A) and we set $f(E_{k\sigma},T)=f(E_k,T)$, $\delta f_\sigma(H_0)=\delta f_\sigma$.

The dominant effect of the field will be the repopulation of the impurity spin orientations through the factor P_c.

In an obvious notation we write

$$\delta H_I(\vec{R}_n) = \tfrac{8}{3}\pi\gamma_e\hbar \sum_c P_c \sigma^c(\vec{R}_n) \quad . \tag{8}$$

We can restate this in terms of the state $c = a$ which has its moment completely parallel to H_0 by incorporating the susceptibility per atom of the impurity χ_d^s

$$\delta H_I(\vec{R}_n) = \tfrac{8}{3}\pi\gamma_e\hbar \frac{\langle \mu_z \rangle}{\mu_{\text{sat}}} \sigma^a(\vec{R}_n)$$

or

$$\delta H_I(\vec{R}_n) = \tfrac{8}{3}\pi \frac{\chi_d^s H_0}{S_{\text{eff}}} \sigma^a(\vec{R}_n) \quad , \tag{9}$$

where $\sigma^a(\vec{R}_n)$ is the spin density for the fully saturated moment and S_{eff} is the apparent spin of the impurity: $\gamma_e\hbar S_{\text{eff}} = \mu_{\text{sat}}$. We express the final result in terms of the change in the Knight shift $\Delta K = \delta H_I/H_0$, which is obtained by the measured positions of the satellite, divided by the pure-metal Knight shift K^0

$$\frac{\Delta K(\vec{R}_n)}{K^0} = -\frac{\chi_d^s(T)}{\chi_s^e}\frac{5}{S_{\text{eff}}}\sum_\sigma m_\sigma \int \rho_1(W_k)\,dW_k \{[n_2^2(kr) - j_2^2(kr)]\sin^2\delta_{2\sigma} - 2n_2(kr)j_2(kr)\sin\delta_{2\sigma}\cos\delta_{2\sigma}\} f(W_k, T) \quad , \tag{10}$$

where χ_s^e is the free-electron susceptibility per atom.

Since the Fermi function serves essentially only as a cutoff for the integral, the entire temperature dependence of the satellite shifts is primarily contained in the prefactor of the impurity susceptibility. This point has been discussed in detail by Boyce and Slichter[16] and is justified on the basis of experimental observations. A second point is that χ_d^s refers properly to the spin part of the total impurity susceptibility as discussed by Abbas, Aton, and Slichter.[17] This distinction is important for impurities that may contain both orbital and spin degrees of freedom (see Sec. IV C).

B. No permanent moment

The details of analysis for this case is presented in Appendix A using the Anderson model picture of moment formation. The result is expressed in terms of a Coulomb repulsion parameter U and the impurity d-level density of states $\rho_d(E_F)$ at the Fermi energy. From Appendix A we have

$$\Delta K(\vec{R}_n)/K^0 = 5\{[n_2^2(k_F r) - j_2^2(k_F r)]\sin^2\delta_2(E_F) - 2n_2(k_F r)j_2(k_F r)\sin\delta_2(E_F)\cos\delta_2(E_F)\}$$
$$-5\frac{\rho_d(E_F)U}{1-\rho_d(E_F)U}\int \frac{\rho_1(W_k)\,dW_k}{\rho_1(E_F)}\Bigg\{[n_2^2(kr) - j_2^2(kr)]\frac{\partial}{\partial E_\sigma}\sin^2\delta_{2\sigma}$$
$$-2n_2(kr)j_2(kr)\frac{\partial}{\partial E_\sigma}(\sin\delta_{2\sigma}\cos\delta_{2\sigma})\Bigg\} f(W_k, T) \quad , \tag{11}$$

where $[\rho_d/(1-\rho_d U)][1/\rho_1(E_F)] = \chi_d^s/\chi_e^s$ and E_σ denotes the energy of the d-wave resonance peak.

The second term dominates the first for those atoms which are nearly magnetic; that is, for $\rho_d U \simeq 1$. We shall consider the application of Eq. (11) to such impurity systems as CuCo and CuV which exhibit a nearly temperature-independent susceptibility.

III. MODEL POTENTIAL

The one-electron formulation given by Eqs. (10) or (11) allows us to compute the copper neighbor Knight shifts once the impurity potential is given. This potential is assumed screened to a constant (zero) for distance r outside a Wigner-Seitz radius, $r_c = 2.67$ bohrs, corresponding to the bottom of the conduction band. For $r < r_c$ the potential is taken to be

$$V(r) = [V_A(r) + C \pm C_{\text{xc}}]e^{-\alpha r} \quad , \tag{12}$$

where $V_A(r)$ is the atomic potential for the free atom given by Herman and Skillman.[18,19] C gives the displacement of this potential relative to the bottom of the band. Since $V_A(r)$ includes an average spin-independent Slater exchange potential, C_{xc} explicitly denotes the spin-dependent d-wave interaction due to the partially filled d levels of the impurity ($\pm$ for up and down spin, respectively). The parameter α indicates screening within the core region itself.

The physical content of the model is most easily visualized by examining the net potential for d-wave electrons shown in Fig. 2. The slightly modified free atomic core potential gives rise to a wave function in the impurity region resembling that of the free atom. The $l = 2$ centrifugal barrier, modified by the screen-

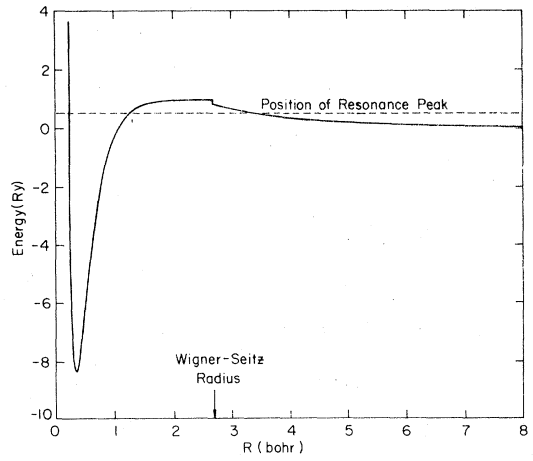

FIG. 2. Model potential for $3d$ electrons vs radial distance from impurity atom. This resultant potential includes the d-wave centrifugal term and gives rise to an effective barrier whose transmission characteristics are determined by the screening parameters in the model.

ing charge, determines the coupling to the host extended states. C and α allow enough freedom in the details of screening that both the position and width of the resulting d-wave scattering "resonances" may be varied. α is expected to be consistent with Fermi-Thomas screening contributed by one electron, lying in the range 0–0.1.

We assume only d-wave scattering is significant in determining the spin-density behavior. A similar potential may be used to examine s- and p-wave scattering although there is no *a priori* reason to expect identical values of C and α to apply to all partial waves.

Once the potential has been parametrized, phase shifts are calculated throughout the conduction band by numerically integrating the radial Schrödinger equation. The Knight shifts at the neighboring copper nuclei are computed with Eqs. (10) or (11). In addition to providing the near-neighbor spin density, an especially important feature of the model is that it enables an identification of the number of d electrons on the magnetic atom that is distinct from that given by the total d-wave screening. Since we know the $l=2$ wave functions $\Psi_{k2\sigma}(r)$ in the core region for each k, we can compute the d-wave charge density as a function of r by integrating over the band

$$\rho_{q3d}(r)=\sum_{\sigma} 5e \int \rho_1(W_k)\,dW_k\,|\psi_{k2\sigma}(r)|^2 f(W_k,T) \ . \tag{13}$$

We find that the *shape* of $\rho_{q3d}(r)$ for the impurity within the core region is the same as that of the free atom. This results because the core potential is nearly the same. Thus, *there is meaning* to the concept of a number of $3d$ electrons determined from the scale factor of $\rho_{q3d}(r)$ compared to that of the free atom. This procedure is demonstrated in the next section.

The three parameters of the model are determined by the measured isotropic Knight shifts and, in the case of the strongly magnetic systems *Cu*Cr, *Cu*Mn, and *Cu*Fe, by the experimental value of the impurity spin determined by fitting the observed temperature dependence of the susceptibility to a Curie-Weiss law (with a g factor of 2). The susceptibility measured spin determined this way includes the exchange-coupled polarization of the extended conduction-electron wave functions. It is this *total S* that should be identified with the difference between the up- and down-spin scattering phase shifts.

The impurity spin is used to impose one constraint on the choice of the model parameters. The two remaining constraints, roughly speaking, are the amplitude and phase of the spin-density oscillations although, as previously mentioned, the spin-density oscillations in the near-neighbor region are not RKKY-like. They exhibit instead a more complicated r dependence (see Sec. V C). Having determined the parameters, impurity resistivities at high temperatures for the alloys with low-Kondo-temperature alloys can be checked via the Friedel formula using the scattering phase shifts at E_F determined by the model. Because Knight shift data are available on the entire series of $3d$ impurities in copper, the comparison of behavior across the periodic table further discriminates against alternative parametrization. A large measure of the success of the model is that it produces solutions that are indeed consistent with all of these considerations. These points will be elaborated in the following section as we apply the model to the experimental data.

IV. COMPARISON WITH ALLOY SYSTEMS

We shall examine several impurity systems in turn. The strongly magnetic alloys (*Cu*Mn, *Cu*Fe, and *Cu*Cr) will be treated first since in these cases the most complete data are available, both in terms of the number of satellites observed and the identification of satellites to specific neighbor shells. In these cases one also has a reasonable basis for the assignment of an impurity spin from susceptibility data. We then discuss *Cu*Co and the remaining copper-$3d$ alloys.

A. *Cu*Mn

Manganese in copper provides the best illustration of the model and is also perhaps the least controversial $3d$ system. The temperature dependence of the susceptibility is nearly a pure Curie law (the Kondo

temperature being well below 1 K) and a majority of measurements agree on an effective moment near $4.9\mu_B(S_{\text{eff}}=2.0)$.[20] Seven magnetic satellites are observed in this system, four of which are unambiguously identified.[7]

The parameters of the model are chosen to give a best (least squares) fit to the data subject to the constraint that the phase shifts at E_F produce the observed impurity spin. This gives an assignment of parameters: $C=0.9664$ Ry, $C_{\text{xc}}=0.1788$ Ry, $\alpha=+0.05$. A comparison of the data with the model is shown in Fig. 3. The corresponding d-wave density of states is determined from the energy dependence of the phase shifts and is shown in Fig. 4. Scattering resonances resembling those of the Hartree-Fock solution of the Anderson model are clearly displayed. Note that the positions and widths are determined entirely from integration of the Schrödinger equation. Thus in this model the levels for up and down scattering will have different widths.

The $l=2$ phase shifts at E_F are 0.15π and 0.95π for up and down spin, respectively. Neglecting s- and p-wave scattering gives an impurity resistivity of 2.14 $\mu\Omega$ cm/at.%.[21] The experimental value is 2.76 $\mu\Omega$ cm/at.% at room temperature.[22]

Computing the integral of the d-wave charge density in the impurity region according to Eq. (13) shows that it corresponds to an assignment of 4.9 d electrons when compared to atomic Mn (see Fig. 5). Since the $l=2$ phase shifts indicate a total d-wave screening of 5.5 d electrons, this implies a charge of 0.6 electrons in the screening cloud outside the impurity atom.

The uncertainties in these results arise from a number of different considerations. By using different restricted sets of satellites to compute model parameters we found a surprisingly small variation in the results as long as at least four satellites were included. The major uncertainties arose from two other sources—the experimental uncertainty in the impurity spin and the magnitude of the hyperfine-coupling constant.

Estimating a ± 0.2 uncertainty in μ_{eff} and a 10% error in the hyperfine coupling yields about a ± 0.2 deviation in the stated number of d electrons. Uncer-

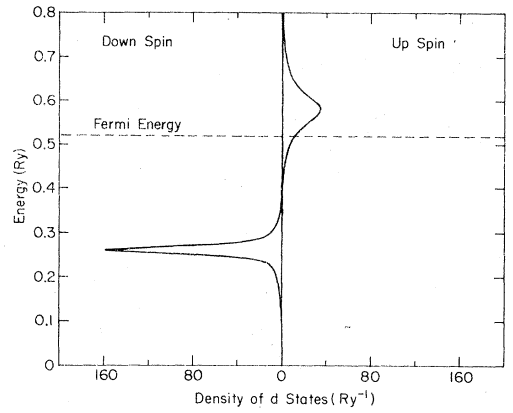

FIG. 4. *Cu*Mn density of d states vs energy above the bottom of the conduction band for up and down spins. Positions, shapes, and widths of resonances are determined entirely from integration of the Schrödinger equation. Thus in this model the resonances for up and down spins have different widths.

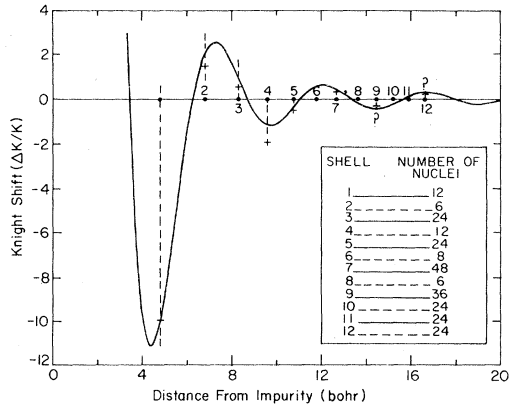

FIG. 3. *Cu*Mn Knight shifts $\Delta K/K$ vs distance from impurity: experiment and theory. Positions of the first twelve nearest-neighbor shells are indicated. Satellites of the fifth and seventh neighbors are assigned on the basis of intensity and those shown at the ninth and twelfth are *not* identified experimentally. The table giving number of nuclei for each shell may explain why certain neighbor shells are not observed.

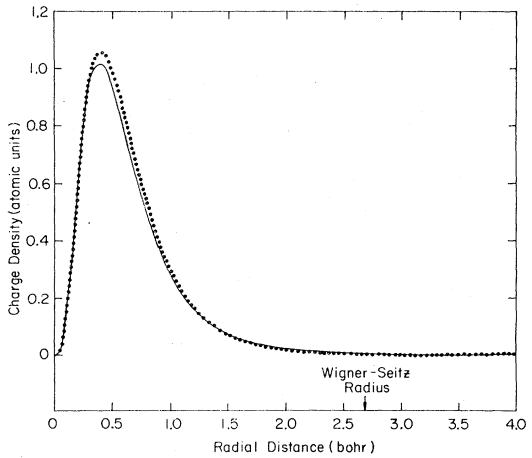

FIG. 5. Total (angular-averaged) d-wave charge density in core region of magnetic atom vs radial distance as given by model for *Cu*Mn (solid line) compared to five Mn $3d$ electrons obtained from Hartree-Fock wave functions of the free atom given in Ref. 45 (dotted line).

tainties in the hyperfine-coupling parameters obviously also effect the overall magnitude of the spin-density oscillations (SDO) determined by the measured Knight shifts. This can lead to a change in the assignment of model parameters that effectively alters the splitting and widths of the scattering resonance displayed in Fig. 3 but by the same factor. The phase shifts of E_F are not appreciably changed. A rather detailed discussion of the hyperfine coupling including intraband enhancement effects has been given by Walstedt and Walker[23] (see also Sec. V C). The 25% smaller coupling that is suggested if K^0 contains a significant orbital component[24] would *increase* the width and splitting of the d levels by roughly that amount but otherwise leave our conclusions the same.

The precise position of the down-spin scattering resonance is also somewhat uncertain. Although significant, the contribution to the SDO from the down-spin scattering is small compared to the contribution from the up-spin scattering nearer the Fermi energy. This makes its exact location less crucial to the fit. The presence of the copper d band 2–3 eV below E_F also is more likely to alter our simple picture significantly in this part of the band.

B. *Cu*Fe

Iron in copper has been a particularly important system because of its conveniently accessible Kondo temperature. The total susceptibility of this system as well as the spin susceptibility determined by the temperature variation of the Knight-shift splittings both show a well-characterized Curie-Weiss behavior with a Weiss temperature, Θ_K, near 28 K. Abbas *et al.*[17] have pointed out that such agreement in the temperature dependence of these two kinds of measurements argues against any significant orbital degrees of freedom for this system. The effective moment is near $3.4\mu_B$.[25] Five magnetic satellites have been observed in the *Cu*Fe systems, three of which have been identified.[6]

Boyce and Slichter[16] attempted an analysis of these data using the interpolation formula of Jena and Geldart. That analysis unfortunately contained a sign error [in their Eq. (27)] which invalidates that analysis. With the correct sign no reasonable fit could be obtained. The interpolation formula is in any case valid only for nearly empty or nearly full scattering levels.[12]

Alloul *et al.*[26] have also performed a calculation of the *Cu*Fe Knight-shift data using the Hartree-Fock magnetic limit of the Anderson model. However, their analysis was based on a postulated shell assignment which was later shown to be incorrect by the single-crystal rotation studies. This example demonstrates the importance of unambiguous satellite identification to extract conclusions from these data.

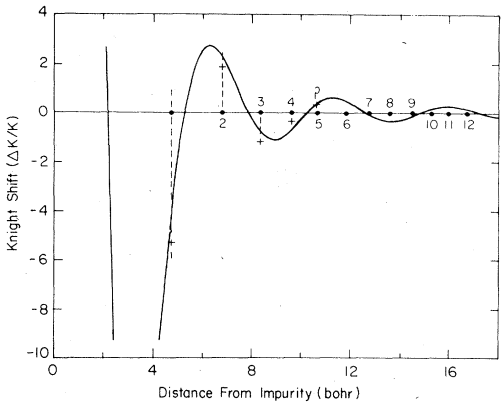

FIG. 6. *Cu*Fe Knight shifts $\Delta K/K$ vs distance from impurity: experiment and theory. Positions of the first twelve nearest-neighbor shells are indicated. The satellite at the fourth-neighbor shell is assigned on the basis of intensity and that shown at the fifth-neighbor shell is *not* identified experimentally.

Assuming a spin only susceptibility ($g = 2$) gives $S = 1.25$. We obtain the fit to the data shown in Fig. 6. The d-wave density of states is shown in Fig. 7. The absence of a down-spin resonance merely indicates that no apparent contribution to the SDO comes from the down-spin scattering. This may indicate a resonance deep in the band obscured by the host d bands. Note that the width of the scattering resonance at E_F agrees closely with the results of *Cu*Mn.

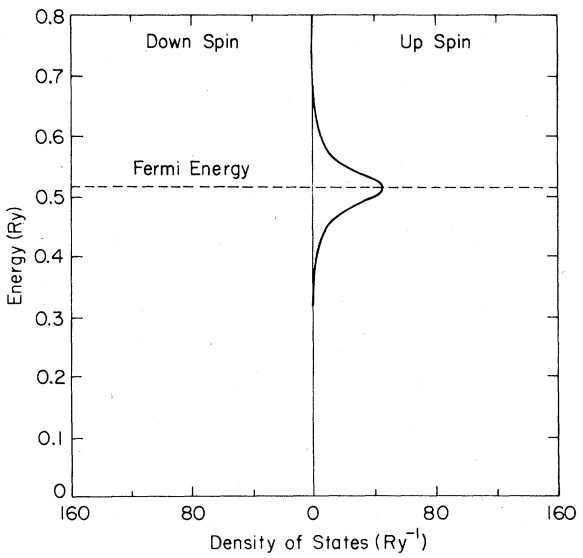

FIG. 7. *Cu*Fe density of d states vs energy above the bottom of the conduction band. The absence of a scattering resonance for down spin in this figure indicates that only a negligible component to the total SDO from down-spin scattering is indicated from the model.

The corresponding model parameters are also similar: $\alpha = 0.05$, $C + C_{xc} = 1.0784$ Ry. The $l = 2$ phase shifts at E_F are near 0.5π and π for up and down spin, respectively, and indicate a high-temperature resistivity of 9.2 $\mu\Omega$ cm/at.% versus an 8.7 $\mu\Omega$ cm/at.% measured value at room temperature.[22]

Computing the integral of the charge density as for *Cu*Mn gives a distribution corresponding to 7.0*d* electrons on the iron impurity. Uncertainties arise as in the case of *Cu*Mn, they lead to a ±0.2 uncertainty in this number.

The nearly integral number of *d* electrons determined in this way for *Cu*Mn and *Cu*Fe strongly suggest an assignment of $3d^5$ and $3d^7$ for these two impurities in copper. By applying a configurational picture to analyze the temperature dependence of the satellite splittings, Abbas *et al.* have presented detailed arguments for the same assignments including the jump of two electrons between Fe and Mn.

C. *Cu*Cr

There is presently some disagreement on the correct characterization of this system. Bulk susceptibility measurements of Monod and Schultz[27] indicated a Curie-Weiss-like behavior with an impurity moment near $3.9\mu_B$ and a Weiss temperature Θ_K of about 1 K. More recent measurements by Vochten *et al.*[28] indicate a temperature-independent component to the bulk susceptibility as well as a marked change in behavior below 12 K. They found the temperature-dependent component could be fit above 12 K by a Curie-Weiss law with $\mu_{\text{eff}} = 3.99\mu_B$ and $\Theta_K = 3.4$ K. Abbas *et al.*[17] have measured the temperature dependence of the *Cu*Cr satellites and found it to exhibit a temperature dependence which fits neither a pure Curie-Weiss law nor is identical to that of the bulk susceptibility. This led them to postulate a configurational model for the Cr impurity along the lines suggested by Hirst[29,30] that includes orbital degrees of freedom.

Aton[8] has studied the satellite spectrum of *Cu*Cr at room temperature and has observed six satellites of which he positively identifies three. We shall attempt to fit these data in a manner similar to *Cu*Mn and *Cu*Fe. However, due to the likelihood of an orbital moment and spin-orbit coupling, there is an *ad hoc* character to treating this system within the context of the present model.

One approach is to proceed as in the case of *Cu*Mn and identify the entire susceptibility with the impurity spin assuming, as had been the original interpretation of this system,[27,29] there are no orbital degrees of freedom. This implies an effective spin near 1.5 and gives a fit to the data shown in Fig. 8 with $C = 1.0204$ Ry, $C_{xc} = 0.0521$ Ry, $\alpha = 0$. The corresponding density of states is shown in Fig. 9. Note the similarity of resonance widths to those of *Cu*Mn and *Cu*Fe. The phase shifts at E_F near 0.2π and 0.8π for up and down spin, respectively, correspond to an impurity resistivity of 6.4 $\mu\Omega$ cm/at.% versus the measured value of 5.5 $\mu\Omega$ cm/at.%.[22]

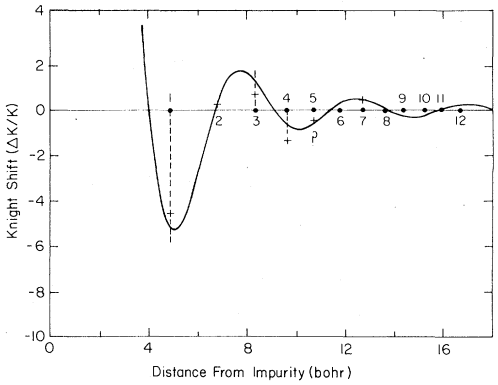

FIG. 8. *Cu*Cr Knight shifts $\Delta K/K$ vs distance from impurity: experiment and theory. Positions of the first twelve nearest-neighbor shell are indicated. The satellites at the seventh-neighbor shell is assigned on the basis of intensity; that shown at the second neighbor is tentatively assigned on the basis of its narrow linewidth. (Whether or not this second-neighbor assignment is correct, the second-neighbor shift is known to be small.) The satellite shown at the fifth-neighbor shell is *not* identified experimentally.

If this system contains both orbital and spin degrees of freedom, the resulting levels will be split by the magnetic field and by spin-orbit coupling. At high temperatures the spin-orbit coupling can be neglected and the spin and orbital susceptibility

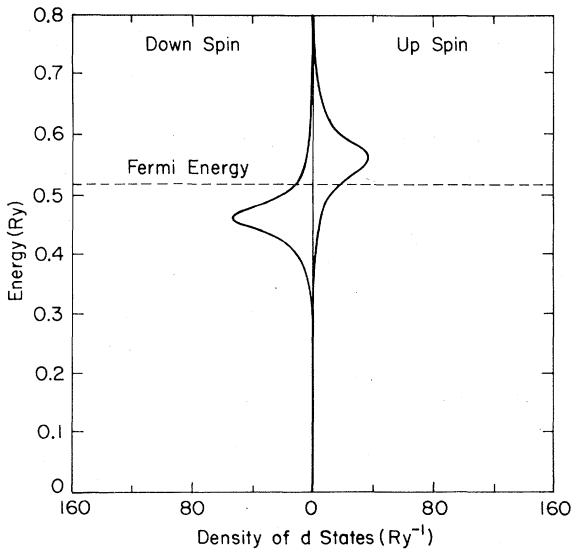

FIG. 9. *Cu*Cr density of *d* states vs energy above the bottom of the conduction band for up and down spins.

separated. If, as suggested by Abbas and co-workers, we further assume that the spatial dependence of the Knight shift depends only on the spin character of the impurity, a one-electron picture *could* perhaps still be applied. Their analysis then indicates that this effective impurity spin would have a value near 1.8 (this is the value of spin that includes the polarization cloud of the conduction electrons).

Such a larger value of spin actually slightly improves the fit to the measured Knight shifts. However, the large uncertainty regarding the impurity spin together with the somewhat poorer quality of fit shown in Fig. 8 makes the assignment of model parameters somewhat less certain. In spite of this, the number of d electrons determined by the model is 4.2 ± 0.3 and shows less variation. This is consistent with a $3d^4$ configurational assignment for the Cr impurity.

D. Discussion of other systems

Although different atomic potentials, $V_A(r)$, were incorporated to generate the model wave functions for each of the alloys discussed so far, a single potential characteristic of the $3d$ impurity, modified suitably by the two screening parameters, is adequate to describe the Knight-shift structure of all three systems. Indeed, the model can be used in this way to generate a relation between the phase shifts at E_F and $\Delta K/K^0$ at the near-neighbor host atoms that accounts reasonably well for all three impurities. Figure 10 displays this relation for the first four neighbors. The vertical scale is the value of the integral in Eq. (10) (with a minus sign) and these curves were obtained by varying the parameter C in the model using a Mn potential for $V_A(r)$ and a fixed value of $\alpha = 0.05$. Curves obtained in this way from other

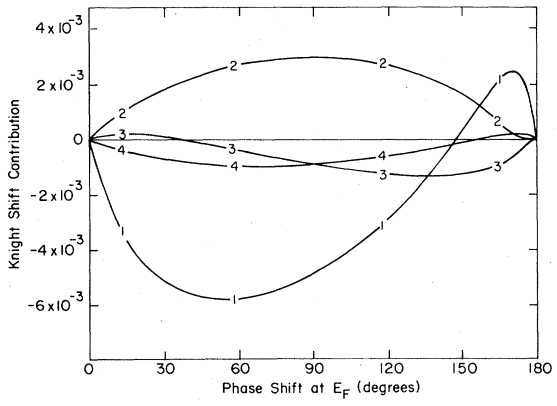

FIG. 10. Contribution to ΔK at first four-neighbor shells vs d-wave scattering phase shift at E_F for an up-spin electron. The vertical scale and application of these curves to compute Knight shifts are explained in the text.

transition-metal atomic potentials or other values of α are nearly indistinguishable from those in Fig. 10 except for a multiplicative scale factor of order unity. Thus one finds the observed trends in the Knight-shift structure as one moves across the Periodic Table mirrored in these curves as the scattering levels more in congruence with the changing value of spin and number of d electrons.

It is of interest to examine the behavior of some of the remaining alloy systems in this context. Satellites have been observed for all of the $3d$ impurities in copper. *Cu*Co has been studied both in powders and single-crystal samples and exhibits three magnetic satellites, two of which have been identified.[6] The remaining alloys have been studied in powders only yielding two satellites[5] for *Cu*V and one each for *Cu*Sc, *Cu*Ti,[31] and *Cu*Ni.[32] Impurity susceptibility measurements are available for all of these systems with the exception of *Cu*Sc.[5]

None of the susceptibility measurements shows a marked temperature dependence. This may indicate a very high Kondo temperature (of, say, greater than 1000 K) or the lack of a permanent moment. Alternatively, it may indicate an impurity ground-state configuration that is nonmagnetic.

We shall examine the first two possibilities for the *Cu*Co system within the context of the model by applying Fig. 10 to fit the observed satellites using Eqs. (10) and (11) in turn. That is, the Knight shifts will be given by

$$\frac{\Delta K(R_n)}{K^0} = \frac{\chi_d^s}{\chi_s^e}\frac{5}{S_{\text{eff}}}\sum_\sigma m_\sigma F_n(\delta_\sigma) \tag{14}$$

for a magnetic impurity and [neglecting the first term in Eq. (11)] by

$$\frac{\Delta K(R_n)}{K^0} = \frac{\chi_d^s}{\chi_s^e} 5U \frac{\partial}{\partial E_\sigma} F_n(\delta_\sigma) \tag{15}$$

for an impurity with no permanent moment. Here $F_n(\delta_\sigma)$ denotes the curve for the nth neighbor shell displayed in Fig. 10 and δ_σ is the phase shift $\delta_{2\sigma}(E_F)$. From Appendix A we have

$$\frac{\partial}{\partial E_\sigma} = \frac{\pi}{5U}\frac{\partial}{\partial \delta_\sigma}$$

with $\delta_+ = \delta_-$. Furthermore, if one identifies the measured susceptibility with χ_d^s, a value of $\rho_d U$ may also be estimated for the spin-induced case by using Eq. (A10) and the results of the model to calculate ρ_d, the value of the d-wave density of states at E_F. We take $\rho_1(E_F) = 0.146\ \text{eV}^{-1}/\text{atom}$.

Because of the uncertainty in the spin susceptibility (due to the possibility of orbital magnetism) and a $\pm 30\%$ uncertainty in the overall scale factor depending on details of screening, we consider agreement to within a constant factor of 2 to be satisfactory. An analysis for *Cu*Co using *either* the spin-split or spin-

TABLE I. Comparison of Knight-shift data for Ti, V, and Co impurities in copper with induced-moment model calculations. Special assumptions and explanation of parameters are explained in the text.

Impurity	χ_d^s/χ_e^s	Assumed levels (phase shift at E_F)	$\rho_d U$	Largest calculated satellites (shell)	Observed satellites (shell)
Ti	32	0.3π	0.40	−0.11 (2)	−0.23
V	96	0.4π	0.72	−0.41 (1) +0.15 (3)	−0.65 +0.22
Co	258	0.85π	0.984	−5.1 (1) +3.3 (2) −0.8 (4)	−1.37 (1) +0.74 (2) −0.28
Co	spin split	$0.69\pi, 0.97\pi$		−0.92 (1) +0.50 (2) −0.19 (3)	−1.37 (1) +0.74 (2) −0.28

induced description yields a fit consistent with its satellite structure and an assignment of parameters indicating eight d electrons (see Table I). The magnitudes of the calculated satellites and apparent value of $\rho_d U$, however, suggest that *Cu*Co is best described as a spin-split system with an effective spin near 0.7. (This conclusion is only valid if the impurity susceptibility does not contain a large orbital component.)

If we *assume* integral configurations for *Cu*Ti and *Cu*V of $3d^2$ and $3d^3$, respectively, and a screening cloud charge of roughly one electron outside the impurity (similar to *Cu*Cr) we may use Eq. (15) to try to predict the satellites of the two systems. The results, also displayed in Table I, indicate there are no apparent inconsistencies in treating *Cu*Ti and *Cu*V as spin-induced impurities with an integral number of d electrons.

V. CALCULATION OF OTHER EXPERIMENTAL QUANTITIES

A. Anisotropic hyperfine shifts

Important additional experimental data on the magnetic structure surrounding the $3d$ impurity in copper comes from the anisotropic components of the Knight-shift tensor obtained in the single-crystal measurements.[6–8] Let us denote this part of the tensor by $\Delta\vec{\mathrm{K}}_D$ where we write the total Knight-shift tensor in component notation as

$$K(\vec{\mathrm{R}}_n)|_{jk} = [K^0 + \Delta K(\vec{\mathrm{R}}_n)]\delta_{jk} + \Delta K_D(\vec{\mathrm{R}}_n)|_{jk} \qquad (16)$$

consisting of the pure copper Knight shift, K^0, the isotropic shift ΔK due to the spin-density oscillations (SDO) as described in Sec. II, and the anisotropic dipolar component. From Eq. (1) we have

$$\Delta\vec{\mathrm{K}}_D \cdot \vec{\mathrm{H}}_0 = \int \left[\frac{\vec{\mathrm{M}}(\vec{r})}{r^3} - \frac{3[\vec{\mathrm{M}}(\vec{r})\cdot\vec{r}]\vec{r}}{r^5} \right] d^3r \ , \qquad (17)$$

where the integral is over all space and $\vec{\mathrm{M}}(\vec{r})$ denotes the total electron-spin magnetization density and $\vec{r}$ is a vector from the copper nucleus in question to a point in the magnetization cloud.

There are two regions of space that give a large contribution to the integral—the region at the magnetic impurity, where $\vec{\mathrm{M}}$ is large, and the region near the Cu nucleus in question, where $1/r^3$ is large. Thus we approximate Eq. (17) by

$$\Delta\vec{\mathrm{K}}_D \cdot \vec{\mathrm{H}}_0 = \frac{\chi_d^s \vec{\mathrm{H}}_0}{R_n^3} - \frac{3(\chi_d^s \vec{\mathrm{H}}_0 \cdot \vec{\mathrm{R}}_n)\vec{\mathrm{R}}_n}{R_n^5} + \int \left[\frac{\vec{\mathrm{M}}(\vec{r})}{r^3} - \frac{3[\vec{\mathrm{M}}(\vec{r})\cdot\vec{r}]\vec{r}}{r^5} \right] d^3r \ , \qquad (18)$$

where the integral goes over the atomic cell containing the Cu nucleus, $\vec{\mathrm{R}}_n$ is the vector from the center of magnetic atom to that nucleus, and χ_d^s is the measured susceptibility of the atom. The first term in Eq. (18) is sometimes referred to as the (direct) dipole term and the second as the pseudodipolar term, although both terms arise from the dipolar part of the hyperfine Hamiltonian in Eq. (1).

Since the impurity susceptibility χ_d^s is known, an experimental value for the cell contribution in Eq. (18) is readily determined from the measured values of $\Delta\vec{\mathrm{K}}_D$. These data are available for three neighbors each of *Cu*Mn and *Cu*Cr, two neighbors of *Cu*Fe, and one of *Cu*Co. The results are tabulated in Table II.

The cell contribution (or pseudodipolar term) can be calculated directly from our model wave functions.

TABLE II. Comparison of the experimental and calculated anisotropic Knight-shift components. The experimental values are taken from Refs. 6–8 with the direct dipole contributions subtracted. There is an ambiguity in the assignment of the measured principle axes to crystallographic directions which generally allow two possibilities for each site. In cases where there is clear agreement between experiment and theory the z axis in the experimental assignment is either the radial direction or close to it.

Neighbor	Cell contribution (direct dipole subtracted) Measured	Calculated
Cr: 1st	+1.76 −1.76 ± 0.08	+1.28
	−0.82 or −0.82 ± 0.08	−0.64
	−0.94 +2.58 ± 0.08	−0.64
3rd	−0.16 ± 0.05	−0.20
	+0.08 ± 0.05	+0.10
	+0.08 ± 0.05	+0.10
4th	+0.155 −0.178 ± 0.010	+0.17
	−0.082 or −0.082 ± 0.010	−0.08
	−0.073 +0.260 ± 0.010	−0.08
Mn: 2nd	−0.303 ± 0.025	−0.57
	+0.152 ± 0.025	−0.28
	+0.152 ± 0.025	−0.28
3rd	−0.041 −0.265 ± 0.010	−0.05
	+0.058 or +0.058 ± 0.010	−0.02
	−0.018 +0.206 ± 0.010	−0.02
4th	+0.180 −0.203 ± 0.015	+0.23
	−0.137 or −0.137 ± 0.015	−0.12
	−0.043 +0.340 ± 0.015	−0.12
Fe: 2nd	−0.134 ± 0.030	−0.36
	+0.067 ± 0.030	+0.18
	+0.067 ± 0.030	+0.18
3rd	−0.35 ± 0.05	+0.23
	+0.23 ± 0.05	−0.12
	+0.14 ± 0.05	−0.12

The factor $1/r^3$ makes the dipolar coupling sensitive to the local details of those wave functions. Thus the free-electron wave functions employed in Sec. II do not suffice, and it is necessary to orthogonalize these to the copper core states. Details of these calculations are given in Appendix B and follow along lines similar to those given by Kohn and Vosko[33] for calculation of the quadrupole coupling near nonmagnetic impurities. These calculations are entirely straightforward and, as they contain no adjustable parameters, form a valuable *independent* experimental check on the results of the model. Our results are tabulated along with the experimental data in Table II.[34] In most cases we account for the axial components of the observed Knight-shift tensor rather well (the only serious discrepancy occurs at the third neighbor of *Cu*Fe).

The large nonaxial character of the Knight-shift tensor for *Cu*Mn and *Cu*Fe is direct evidence of the nonuniform part of the lattice potential. Boyce and Slichter have suggested it may arise from a crystal-field splitting of the d-wave scattering resonances.[16] We have investigated this approach by incorporating a small crystal-field parameter in $V(r)$ [Eq. (12)] but find that although this will give rise to a nonaxial coupling, the asymmetries can be at most a few percent, much smaller than actually observed (see Appendix B).

An alternate explanation is that if significant scattering due to the impurity occurs deep in the band, multiple scattering may arise from the copper d levels, an effect we have neglected. Thus, since the impurity scattering is spin dependent, the Cu secondary scattering will produce nonspherical spin-density

oscillations. Along these lines we note that for *Cu*Cr where neither "resonance" is expected to lie deep within the band (see Fig. 8) the data show a Knight-shift anisotropy that is, indeed, almost purely axial.

The discrepancy at the third neighbor of *Cu*Fe is harder to reconcile. We note a recent measurement in the *Cu*Fe system at low temperature has suggested a different origin for the satellite splittings in this system than the dipolar hyperfine coupling alone.[35] On the other hand, a large distortion from spherical SDO is certainly apparent at the *Cu*Fe third neighbor from the experimental data; perhaps the lack of agreement with our simple calculation for this system is not surprising.

B. Electric quadrupole coupling

Electric quadrupole couplings have been determined for a variety of the copper-3*d* systems at specific neighbor shells. In particular, Aton has determined the complete quadrupole tensor for three neighbors each of *Cu*Mn and *Cu*Cr. Quadrupole couplings are, in general, quite difficult to calculate. Stakelon and Slichter[6] have pointed out that there exists a basic relationship between the *d*-wave electron contribution to the quadrupole coupling and the pseudodipolar hyperfine coupling

$$\delta H_{\rm PD} = \frac{\chi_d^s H_0}{S_{\rm eff}} \frac{1}{2} \frac{\nu_{zz}(-) - \nu_{zz}(+)}{2.79 \times 10^{-18}} , \tag{19}$$

where $\nu_{zz}(+)$ and $\nu_{zz}(-)$ refer to the separate contributions to the quadrupole couplings from the up- and down-spin *d*-wave conduction-electron scattering, respectively. As written, their formula relates $\delta H_{\rm PD}$ in gauss directly to ν_{zz} in MHz.

Equation (19) ignores contributions to the electric field gradient (EFG) from the *s*- and *p*-wave scattering as well as strain effects due to the mismatch of the impurity size to the host lattice. Sagalyn and Alexander have shown that, in addition, the region outside the impurity "cell" contributes rather significantly to the EFG, often as much as from the impurity region itself for the near-neighbor shells, as a result of antishielding enhancement.[36] Thus order of magnitude agreement is probably all that can reasonably be expected from Eq. (19) and this is verified by calculation. Table III shows results for *Cu*Cr and *Cu*Mn.

Although more detailed calculations are clearly needed to obtain a quantitative comparison with the data, this simple calculation indicates that the distortion of the lattice around 3*d* impurities in copper is not large. Indeed, estimates of this distortion for nonmagnetic fourth-row impurities in copper from x-ray data provides a correction to the nearest-neighbor distance of only one or two percent and a correction to the electronic component of the EFG at the first neighbor of less than 10%.[36,37]

TABLE III. Quadrupole splittings for *Cu*Cr and *Cu*Mn data from Refs. 7 and 8 compared to that calculated via Eq. (17) from the cell contribution to the anisotropic Knight-shift tensor. The sign of the experimental value of ν_{zz} is not determined.

Neighbor	Quadrupole moment ν_{zz} (MHz) Measured	Calculated
Cr: 3rd	0.198 ± 0.003	−0.99
4th	0.094 ± 0.005	−0.30
Mn: 2nd	0.281 ± 0.004	1.26
3rd	0.106 ± 0.003	−0.43
4th	0.187 ± 0.004	−0.17

C. Asymptotic behavior: NMR linewidth studies

We finally should comment briefly on the connection between our results which are based strictly on the near-neighbor behavior of the spin density and the asymptotic behavior discussed by other workers based on studies of the host copper NMR linewidth as a function of magnetic impurity concentration. We shall restrict this discussion to the "spin-split" alloy systems.

In the asymptotic limit Eq. (10) assumes the familiar RKKY form

$$\frac{\Delta K(R_n)}{K^0} = \frac{\chi_d^s(T)}{\chi_e^s} \frac{\Omega}{S_{\rm eff}} \frac{5}{8\pi^2} \sin(\delta_{2+} - \delta_{2-}) \times \frac{\cos(2k_F R_n + \phi)}{R_n^3} , \tag{20}$$

where δ_{2+} and δ_{2-} are the phase shifts for *d*-wave scattering at E_F for up and down spins, respectively, and where $\phi = \delta_{2+} + \delta_{2-}$. Thus, in the asymptotic limit, the spin density is completely characterized by the phase shifts at E_F.

An important question is at what distance Eq. (20) becomes valid. We can illustrate this using the model determined spin density for *Cu*Mn (see Fig. 2) cast into the form

$$\sigma(r) = A(r) \cos[2k_F r + \phi(r)]/r^3 , \tag{21}$$

where

$$\lim_{r\to\infty} A(r) \equiv A_\infty = \frac{\langle S_z \rangle}{S_{\rm eff}} \frac{5}{8\pi^2} \sin(\delta_{2+} + \delta_{2-})$$

in the asymptotic limit.

In Fig. 11 we plot $A(r)/A_\infty$ and ϕ as a function of r for *Cu*Mn. The variation of both parameters is seen to be considerable for $r \lesssim 50$ bohrs or for the

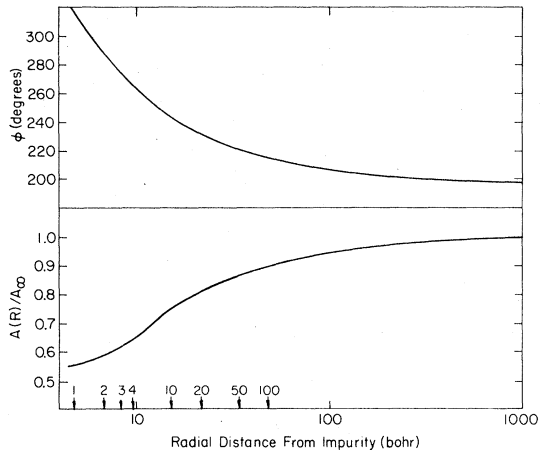

FIG. 11. Amplitude and phase of the spin density for *Cu*Mn vs radial distance from impurity showing the approach of the spin density to its asymptotic behavior. The radial distances to specific neighbor shells are indicated. Note the large distance over which the spin density demonstrates "preasymptotic" behavior.

first 100 shells of neighbors.

In this region the SDO have a significantly smaller amplitude than is predicted by the asymptotic formula. At very large distances the amplitude will also be decreased due to various sources of scattering of the conduction electrons which lead to an exponential damping of the RKKY oscillations. This effect has been estimated in several cases for copper alloys and indicates a damping length on the order of a few hundred bohrs.[38,39]

A detailed discussion of the interpretation of NMR line shape data from RKKY and dipolar broadening has been given by Walstedt and Walker[39] (WW), Alloul, Darville, and Bernier[26] (ADB), and others. WW find a simple relationship between the measured half-width at half-height, $\langle \Delta H \rangle$, of the copper NMR line and the amplitude of the hyperfine-field oscillation $A_{\rm hf}$

$$\langle \Delta H \rangle = 16\pi A_{\rm hf} c/3a^3 \ , \tag{22}$$

where c is the impurity concentration and a is the fcc lattice constant.

$A_{\rm hf}$ is related to the amplitude A of the spin density defined in Eq. (21) via the hyperfine-coupling constants. There is some lack of agreement among different workers as to the precise value of this coupling depending on the assumed values of the density of states at E_F for conduction electrons, the spin susceptibility χ_e^s and Knight shift K^0 of the copper host, and inclusion of host band exchange enhancement factors. The hyperfine coupling used to calculate satellite positions in Sec. IV,

$$\delta H_l(R_n) = (K^0\Omega/\chi_e^s)\gamma_e\hbar\sigma(R_n) \ ,$$

TABLE IV. Comparison of broadening coefficient data from Ref. 26 with that calculated from the spin density predicted from the model in the asymptotic limit. The numbers in parentheses are for the smaller hyperfine coupling suggested by some workers. Units for the broadening coefficient W are given in kG (impurity concentration)$^{-1}$.

Alloy system	W expt.	Calc.	Assumed $\mu_{\rm eff}$
*Cu*Mn	178 ± 20 136 ± 15	217 (163)	4.9
*Cu*Cr	240 ± 50	467 (350)	3.9
*Cu*Fe	450 ± 60	590 (442)	3.4

with $\chi_e^s = 1.55 \times 10^{-29}$ emu/atom,[40] and where Ω denotes the atomic volume, agrees numerically with that employed by WW *except* for the question of an orbital component to K^0 (we have assumed *no* orbital component).

We calculate the so-called broadening coefficient, $W = \langle H \rangle / c \langle S_z \rangle$, as given by Eqs. (21) and (22) and compare it in Table IV with measured values of ADB for these systems. Since the broadening does not depend on the phase of the SDO, it is completely determined by the difference in scattering phase shifts for up and down scattering, i.e., by the impurity spin.

These predicted values are in general somewhat higher than those observed although generally in agreement, particularly for the 25% smaller hyperfine coupling indicated by Walstedt and Yafet.[24] The uncertainties of the measured and predicted values are, in any case, rather significant. A prediction of the too large a broadening coefficient is consistent with the damping of RKKY oscillations at large distances and the smaller amplitude of the SDO in the preasymptotic region.

VI. CONCLUSIONS AND DISCUSSION

The model put forward in this paper has been shown to be very successful toward describing the near-neighbor Knight-shift data for the iron-group impurities in copper. Although some of our results do not differ in certain respects from other attempts to describe specific systems such as *Cu*Mn, the present model is particularly useful because it: (i) accounts for the entire series of $3d$ impurities reasonably well within one simple theory, including cases where the impurity does not possess a permanent magnetic moment, (ii) accounts quantitatively for the anisotropic Knight-shift data of these alloys, (iii) allows for a unique identification of the number of $3d$

electrons which supports arguments for a configurational picture of these impurity systems, and (iv) produces results that are reasonably consistent with a wealth of existing experimental data including impurity resistivities, quadrupole coupling, and NMR linebroadening measurements. In this context we also wish to mention one recent measurement which provides additional verification of the results for *Cu*Mn. Through de Haas-van Alphen measurements of this system, Hendel[41] has been able to obtain directly the scattering phase shifts at E_F for up- and down-spin electrons. His analysis gives $\delta_\uparrow(E_F)=0.18\pi$ and $\delta_\downarrow(E_F)=0.88\pi$ to within 10% accuracy. The proximity of particularly the up-spin phase shift to our deduced value of 0.15π is a rather gratifying result.

In spite of such success, a couple of shortcomings should be discussed. These concern the band structure of the host and the configurational character of the impurity. The former, it is believed, is largely responsible for the remaining discrepancies in the fit of the SDO data to the theory and for the nonaxial character of the anisotropic shifts. Both kinds of discrepancies exist for even the presumably simple impurity moment system *Cu*Mn. A more complete calculation along the lines presented by the current model which includes secondary scattering from the copper *d* bands could presumably account for these differences.

The latter problem, that of configurational degrees of freedom, presents a more serious difficulty. The simple approach presented for *Cu*Cr is not entirely satisfactory. The complex behavior that may arise when the mixing interaction is of the same order as some of the configurational splittings are totally beyond the scope of our model and have been discussed to some degree by Cogblin and Blandin,[42] Hirst,[29,30] Barnes,[43,44] and others. Proper theoretical treatment of such systems remains one of the outstanding problems in understanding the $3d$ impurity in metals.

Evidence for the configurational nature of these systems, is presently rather compelling.[1,2,17] Our own determination of nearly integral assignments of $3d$ electrons supports this viewpoint. One immediate question often arises, therefore, regarding how to reconcile such configurational models, with energy splittings often much less than 0.1 eV for the impurity atom, while also subscribing to a picture of $3d$ scattering resonances which indicate, in our model as well as those of previous workers, an s-d exchange interaction of 1–3 eV. To address this question in part we argue along the lines that have already been put forward by Hirst[29,30] but probably need to be reemphasized.

The widths of the scattering levels represent the problem as viewed by the conduction electrons. We may visualize that these hop on and off the impurity atom and that this mostly takes place in the $4s$ and $4p$ states. For an electron to hop onto a $3d$ state, in fact, is an exceptional event and it corresponds to a *change* in the $3d$ configuration. Thus it hops off very rapidly which results in the large linewidth. In the one-electron model, the ability of an electron to penetrate and then depart is determined by the tunneling barrier in the *d*-wave potential.

From the viewpoint of the impurity, on the other hand, the $3d$ configurational ground state is very long lived. When an electron hops on, it causes a precession of the total angular momentum but, as these events are rare, this perturbation of the $3d$ configurational ground state is small. Indeed, the effect on the $3d$ ground-state levels is on the order of kT_K, which is quite small for Mn, Fe, or Cr in copper. It then makes perfect sense to discuss configurational spin-orbit splitting which may be on the order of only a few tens of wave numbers.

To properly reconcile these points, a more complete many-body treatment of these systems is clearly needed. However, the general applicability of the present model to account for a wide range of experimental properties of first-row transition-metal impurities in copper seems amply demonstrated.

ACKNOWLEDGMENTS

We wish to thank William L. McMillan for the initial suggestion which led to our approach and gratefully acknowledge many discussions and suggestions from John D. Dow. We also enjoyed helpful discussions with T. Aton and D. Abbas. This work was supported by the U.S. Energy Research and Development Administration Contract No. EY-C-02-1198 and by the National Science Foundation Grant No. DMR-73-07661.

APPENDIX A: SATELLITE SHIFTS FOR IMPURITIES POSSESSING NO PERMANENT MOMENT

In this appendix we detail the calculation of satellite shifts for impurities that are not spin split, but which will have an induced moment in the presence of the applied field H_0. We treat this problem within the notation of the Hartree-Fock solution to the Anderson model[10] and denote the positions of the conduction-electron-scattering resonance peaks by

$$E_\sigma = E_0 + U\langle n_{-\sigma}\rangle \ , \tag{A1}$$

where E_0 is the unperturbed resonance position, U is the Coulomb repulsion parameter, and $\langle n_\sigma\rangle$ is the occupation of the level of spin σ given by

$$\langle n_\sigma\rangle = (5/\pi)\delta_\sigma(E_f) \ , \tag{A2}$$

where $\delta_\sigma(E_F)$ denotes the *d*-wave phase shift at the

Fermi energy. We let ρ_σ denote the extra density of d electrons for spin σ at E_F.

Application of H_0 causes a net spin polarization due to the difference in the Fermi function f of two electrons in the same spatial state but of opposite spin. For convenience in the calculation we adopt the notion of a spin-dependent Fermi energy

$$f(W_{k\sigma},E_F)=f(W_k,(E_F-\gamma_{\rm eff}H_0m_\sigma))$$
$$\equiv f(W_k,E_{F\sigma}) ,$$

where

$$E_{F\sigma}=E_F-\gamma_{\rm eff}\hbar H_0m_\sigma . \tag{A3}$$

That is, this approach leaves the electron energy independent of spin orientation and absorbs the spin-dependent energy into E_F.

We next compute the change in $\langle n_\sigma\rangle$ due to H_0. From Eq. (A1) we write

$$\delta E_\sigma=\delta E_0+U\delta\langle n_{-\sigma}\rangle$$

and also have

$$\delta\langle n_\sigma\rangle=\rho_\sigma\delta E_{F\sigma}-\rho_\sigma\delta E_\sigma ,$$

where $\delta E_{F\sigma}=-\gamma_{\rm eff}\hbar m_\sigma H_0$.

Since H_0 should produce nearly no change in the number of d electrons, we postulate

$$\delta\langle n_+\rangle+\delta\langle n_-\rangle=0 .$$

Thus,

$$\delta\langle n_\sigma\rangle=\frac{\rho_\sigma(\delta E_{F\sigma}-\delta E_0)}{1-\rho_\sigma U} .$$

For the nonspin-split case $\delta E_0=0$. Also $\rho_+\simeq\rho_-\equiv\rho_d$. Therefore,

$$\delta\langle n_\sigma\rangle=-\gamma_{\rm eff}\hbar H_0m_\sigma\rho_dU/(1-\rho_dU) . \tag{A4}$$

Since there is zero average moment for $H_0=0$, the average spin magnetic moment per impurity, $\langle\mu_z\rangle$, when the field is applied is

$$\langle\mu_z\rangle=-\sum_\sigma\gamma_e\hbar m_\sigma\delta\langle n_\sigma\rangle$$
$$=\tfrac{1}{2}\gamma_e\gamma_{\rm eff}\hbar^2\rho_dH_0/(1-\rho_dU) ,$$

which gives us the usual result for the impurity spin susceptibility

$$\chi_d^s=\tfrac{1}{2}\gamma_e\gamma_{\rm eff}\hbar^2\rho_d[1/(1-\rho_dU)] . \tag{A5}$$

The enhancement factor, $1/(1-\rho_dU)$, becomes infinite as $\rho_dU\to1$, representing the occurrence of spontaneous magnetization.

To compute $\delta H_l(\vec{\rm R}_n)$ as in Eq. (7), we omit "c" and the sum over "c," and replace the Fermi function using Eq. (A3). This gives

$$\delta H_l(\vec{\rm R}_n)=-\tfrac{8}{3}\pi\gamma_e\hbar\frac{5}{\Omega}\sum_\sigma m_\sigma\int\rho_1(W_k)dW_k\{[n_2^2(kr)-j_2^2(kr)]\sin^2\delta_{2\sigma}(H_0)$$
$$-2n_2(kr)j_2(kr)\sin\delta_{2\sigma}(H_0)\cos\delta_{2\sigma}(H_0)\}f(W_k,E_{F\sigma}) . \tag{A6}$$

We next expand $\delta_{2\sigma}(H_0)$ and $f(W_k,E_{F\sigma})$ in the magnetic field using Eqs. (A3) and (B4), keeping only terms linear in H_0

$$f(W_k,E_{F\sigma})=f(W_k,E_F)+(\partial f/\partial W_k)\gamma_{\rm eff}\hbar H_0m_\sigma .$$

To good approximation $\partial f/\partial W_k\cong-\delta(W_k-E_F)$ and hence we get

$$\delta H_l(\vec{\rm R}_n)=\tfrac{8}{3}\pi\tfrac{1}{2}\gamma_e\gamma_{\rm eff}\hbar^2H_0\frac{5}{\Omega}\Bigg[[(n_2^2-j_2^2)\sin^2\delta_2(E_F)-2n_2j_2\sin\delta_2(E_F)\cos\delta_2(E_F)\rho_1(E_F)]$$
$$-\frac{\rho_dU}{1-\rho_dU}\int_0^{E_F}\rho_1(W_k)\Bigg[(n_2^2-j_2^2)\frac{\partial}{\partial E_\sigma}\sin^2\delta_2$$
$$-2n_2j_2\frac{\partial}{\partial E_\sigma}(\sin\delta_2\cos\delta_2)\Bigg]dW_k\Bigg] . \tag{A7}$$

To get our final result given by Eq. (11) we note that

$$K^0=\tfrac{8}{3}\pi|\psi(\vec{\rm R}_n)|^2_{E_F}\chi_s^e ,$$

where

$$\chi_s^e=\gamma_e\tfrac{1}{2}\gamma_{\rm eff}\hbar^2\rho_1(E_F) \tag{A8}$$

and that for free electrons we have

$$\Omega|\psi(\vec{\rm R}_n)|^2_{E_F}=1 .$$

As discussed in Sec. II, by calculating both the satellite and pure-metal shifts in the free-electron approximation and taking the ratio, we should arrive at a reasonably accurate result.

Evaluation of the derivatives in Eq. (A7) or Eq. (11) is most easily carried out using

$$\frac{\partial}{\partial E_\sigma} = \frac{1}{U}\frac{\partial}{\partial \langle n_{-\sigma}\rangle} = \frac{\pi}{5U}\frac{\partial}{\partial \delta_{-\sigma}} \quad . \tag{A9}$$

Furthermore, the prefactors can be cast into a more recognizable form by noting that from Eqs. (A5) and (A8) we have

$$\frac{\chi_d^s}{\chi_s^e} = \frac{\rho_d}{\rho_1(E_F)(1-\rho_d U)} \quad .$$

APPENDIX B: CALCULATION OF ANISOTROPIC SHIFTS

In this appendix we outline the method for calculating the effective dipole field, $\delta\vec{H}_D$, arising from the cell region surrounding the copper nucleus itself, as defined in Sec. V A. Denoting the second term in Eq. (1) by $\mathcal{H}_D$ we proceed as in Sec. II and define the apparent nuclear-spin Hamiltonian by

$$-\vec{\mu}_N \cdot \delta\vec{H}_D(\vec{R}_n) = \langle Im_I|\mathcal{H}_d(I)|Im_I\rangle \quad ,$$

where

$$\mathcal{H}_d(I) = \sum_{\alpha\sigma}\langle\alpha\sigma|\mathcal{H}_D|\alpha\sigma\rangle f(E_{\alpha\sigma},T) - \sum_{\beta\sigma}\langle\beta\sigma|\mathcal{H}_D|\beta\sigma\rangle f(E_{\beta\sigma},T) \quad . \tag{B1}$$

For purposes of convenience with the notation we have not included the superscript "c" as in Sec. II to label the moment orientation but rather incorporate the appropriate susceptibility factor in our final result. Equation (B1) therefore really describes the fully saturated "a" configuration. $|Im_I\rangle$ denotes the nuclear-spin wave function.

The wave functions $|\alpha\sigma\rangle$ and $|\beta\sigma\rangle$ will denote orthogonalized plane-wave states in the presence of the impurity and for the pure metal, respectively. That is

$$|\alpha\sigma\rangle = \frac{1}{N_{\alpha\sigma}}\left(\psi_{\alpha\sigma} - \sum_{\Gamma p} a_{\alpha\sigma\Gamma p}|\Gamma p\,\sigma\rangle\right) \quad , \tag{B2}$$

where $|\Gamma p\,\sigma\rangle$ refers to the Γth atomic core function on the pth atom, $\psi_{\alpha\sigma}$ represents the free-electron plane-wave state, and the a coefficients are the overlap integrals. $N_{\alpha\sigma}$ is the normalization

$$N^*_{\alpha\sigma}N_{\alpha\sigma} = 1 - \sum_{\Gamma p} a_{\alpha\sigma\Gamma p}a^*_{\alpha\sigma\Gamma p} \quad .$$

In combining Eqs. (B1) and (B2) the terms that are quadratic in the overlap coefficients will dominate in the "cell" region (see Sec. V) and we obtain

$$\langle\alpha\sigma|\mathcal{H}_D|\alpha\sigma\rangle_{\text{cell}} \simeq \frac{1}{N^*_{\alpha\sigma}N_{\alpha\sigma}}\sum_{\Gamma\Gamma',p} a^*_{\alpha\sigma\Gamma p}a_{\alpha\sigma\Gamma' p}\langle\Gamma p\,\sigma|\mathcal{H}_D|\Gamma' p\,\sigma\rangle \quad , \tag{B3}$$

which contains cross terms between different atomic states, Γ and Γ'. However, in the sum over p only the atom $p=n$ containing the nuclear moment μ_N will appear and we may drop the p summation. This gives us

$$H_d(I) = \sum_{\Gamma,\Gamma',\sigma}\langle\Gamma\sigma|H_D|\Gamma'\sigma\rangle \times\left(\sum_\alpha \frac{1}{N^*_{\alpha\sigma}N_{\alpha\sigma}}a^*_{\alpha\sigma\Gamma n}a_{\alpha\sigma\Gamma' n}f(E_{\alpha\sigma},T) - \sum_\beta \frac{1}{N^*_{\beta\sigma}N_{\beta\sigma}}a^*_{\beta\sigma\Gamma n}a_{\beta\sigma\Gamma' n}f(E_{\beta\sigma},T)\right) \quad . \tag{B4}$$

Note that $\langle\Gamma\sigma|\mathcal{H}_D|\Gamma'\sigma\rangle$, which represents the matrix element of the dipole Hamiltonian evaluated between the copper core states Γ and Γ', is independent of the particular site n.

The core functions are taken from Hartree-Fock calculations for atomic copper[45] where $\Gamma=(NLM)$ will denote the usual atomic quantum numbers. $\alpha=(klm)$ labels the free-electron states. Of the nonvanishing terms, those with $\Gamma=\Gamma'=(3pM)$ are found to give the largest contribution to the dipole coupling. The next largest comes from the $\Gamma=3p$, $\Gamma'=2p$ like terms followed by the $2p$-$2p$, $3d$-$3d$, and $3d$-Ns terms. It is sufficient to keep only the $3p$-$3p$ and $3p$-$2p$ cross terms for a reasonable estimate of $\mathcal{H}_d(I)$.

We further illustrate the method by evaluating $3p$-$3p$ cross term. It is convenient to separate out the spin dependence of the copper core functions and define

$$\mathcal{H}_d(I,S) = \sum_{\sigma,M}\langle\mathcal{H}_d\rangle_{MM}A^\sigma_{MM}(\vec{R}_n) \quad ,$$

where

$$\langle\mathcal{H}_d\rangle_{MM} = \langle 3pM|\mathcal{H}_d|3pM\rangle \quad . \tag{B5}$$

For p core functions, $\mathcal{H}_d(I,S)$ is then easily expressed in terms of the nuclear- and electron-spin operators, e.g.,

$$\langle\mathcal{H}_d\rangle_{zz} = \gamma_e\gamma_n\hbar^2\langle 1/r^3\rangle\tfrac{1}{5}(4I_zS_z - 2I_xS_x - 2I_yS_y) + \mathfrak{C} \quad , \tag{B6}$$

where $\mathfrak{C}$ represents cyclic permutation terms and $\langle 1/r^3\rangle$ is the expectation value of $1/r^3$ for the $3p$ atomic copper wave function and we take $\hat{z}$ as the direction from the magnetic impurity to the copper nucleus in question.

The term $A^\sigma_{MM}(R_n)$ represents the quadratic factor in the a overlap coefficients [the term in brackets in Eq. (B4)] and can be expressed in terms of the

TABLE V. Relative contributions to anisotropic Knight-shift tensor component $\Delta K_0|_{zz}^{\text{cell}}$ at *Cu*Mn fourth neighbor from terms in Eq. (B4).

	$3p$-$3p$	$3p$-$2p$
$A_{zz}^{\uparrow}$	-2.50×10^{-4}	-12.6×10^{-6}
$A_{zz}^{\downarrow}$	$+1.22\times10^{-4}$	7.0×10^{-6}
$A_{xx}^{\uparrow}=A_{yy}^{\uparrow}$	0.19×10^{-4}	$+1.3\times10^{-6}$
$A_{xx}^{\downarrow}=A_{yy}^{\downarrow}$	-0.03×10^{-4}	-0.3×10^{-6}
$\langle 1/r^3\rangle$	$83.0a_0^{-3}$	$-224a_0^{-3}$
Contribution to $\Delta K_0\|_{zz}^{\text{cell}}$	7.38×10^{-4}	$(-1.04\times10^{-4})\times2$

model wave functions given by Eq. (6) as

$$A_{MM}^{\sigma}=\sum_{m}\int dW_k\rho_1(W_k)\xi_{mM}^2\{[J^{mM}(R_n,k)\cos\delta_{2\delta}(k)-N^{mM}(R_n,k)\sin\delta_{2\sigma}(k)]^2-[J^{mM}(R_n,k)]^2\}f(W_k,T)\ , \tag{B7}$$

where J and N are the overlap integrals of the appropriately normalized spherical function $j_2(kr)Y_{2m}$ and $n_2(kr)Y_{2m}$ with the copper $3p$ core function $|3pM\sigma\rangle$ located at R_n. These integral functions are readily evaluated using the Löwdin alpha expansion. The coefficients ξ_{mM}^2 come from integrating the angular functions and are replaced by a simple Kronecker delta when the same axis of quantization is chosen for both m and M.

Components of the Knight-shift tensor are obtained from Eq. (B5) by considering the application of a static field and evaluating $H_d(I,S)$ between the appropriate spin functions. The z axis joining the impurity to the copper nucleus is a principle axis of the tensor and it is axially symmetric about this axis. Incorporating the moment polarization factor, $\chi_d^s/\gamma_e\hbar S_{\text{eff}}$, we obtain the result

$$\Delta\vec{K}_D(\vec{R}_n)|_{zz}^{\text{cell}}=-\frac{\chi_d^s}{S_{\text{eff}}}\left\langle\frac{1}{r^3}\right\rangle 3p\sum_{\sigma}m_\sigma\tfrac{1}{5}(4A_{zz}^{\sigma}-2A_{xx}^{\sigma}-2A_{yy}^{\sigma})+\mathfrak{C}\ . \tag{B8}$$

For the final result, one must sum up the contributions to the components of the Knight-shift tensor from each of the core terms in Eq. (B4). Results of these calculations of the *Cu*Mn fourth neighbor (using the model potential parameters determined in Sec. IV A) are tabulated in Table V to indicate the relative contributions of the $3p$-$3p$ and $3p$-$2p$ cross terms in Eq. (B4). Note that the tabulated values of the anisotropic shifts in Sec. V have been divided by the pure copper Knight shift, K^0, since the experimental data are given that form.

This formalism is easily adapted to incorporate a crystal-field dependence of the model by letting the phase shifts $\delta_{2\sigma}$ depend on m in Eq. (7) (that is, on the symmetry of the scattered wave with respect to the cubic axes of the crystal). In that case $A_{xx}^{\sigma}\neq A_{yy}^{\sigma}$ and one indeed obtains a nonaxial tensor. The asymmetry parameter η_K is given by

$$\eta_K=\sum_{\sigma}\frac{|3A_{xx}^{\sigma}-3A_{yy}^{\sigma}|}{2A_{zz}^{\sigma}-A_{xx}^{\sigma}-A_{yy}^{\sigma}}\ .$$

However, as is apparent from the relative magnitude of A_{xx}^{σ} to A_{zz}^{σ} in Table V, the maximum size crystal-field splittings one might expect gives an asymmetry for the fourth neighbor of roughly 5%. Thus this approach does not account for the 52% *measured* asymmetry of the *Cu*Mn fourth neighbor.

*Now at: Bell Laboratories, Murray Hill, N.J. 07974.

[1]R. Dupree, R. E. Walstedt, and W. W. Warren, Jr., Phys. Rev. Lett. 38, 612 (1977).
[2]A. Narath, Phys. Rev. B 13, 3724 (1976).
[3]J. B. Boyce and C. P. Slichter, Phys. Rev. Lett. 32, 61 (1972).
[4]H. Alloul, P. Bernier, H. Launois, and J. P. Pouget, J. Phys. Soc. Jpn. 30, 101 (1971).
[5]For a summary of satellite data of $3d$ impurities in copper, see D. M. Follstaedt, D. Abbas, T. S. Stakelon, and C. P. Slichter, Phys. Rev. B 14, 47 (1976).
[6]Thomas S. Stakelon and Charles P. Slichter, Phys. Rev. B

14, 3793 (1976).
[7]T. J. Aton, T. S. Stakelon, and C. P. Slichter, Phys. Rev. B 18, 3337 (1978).
[8]T. J. Aton, T. S. Stakelon, and C. P. Slichter (unpublished).
[9]J. Friedel, Adv. Phys. 3, 446 (1954); Nuovo Cimento Suppl. 7, 287 (1958).
[10]P. W. Anderson, Phys. Rev. 124, 41 (1961).
[11]P. Jena and D. J. W. Geldart, Phys. Rev. B 7, 439 (1973).
[12]We have compared the results of the interpolation formula of Ref. 11 with the universal satellite shift curves of Fig. 10 generated by our model (see Sec. IV D). This indicates general validity of the interpolation formula for levels less than 10% full (or empty) and large deviations beyond those limits.
[13]An earlier account of our model has been given, see J. David Cohen and Charles P. Slichter, Phys. Rev. Lett. 40, 129 (1978); see also, J. David Cohen and Charles P. Slichter, J. Appl. Phys. 49, 1537 (1978).
[14]H. Alloul, J. Phys. F 4, 1501 (1974).
[15]J. C. Parlebas, J. Phys. F 4, 1392 (1974).
[16]James B. Boyce and C. P. Slichter, Phys. Rev. B 13, 379 (1976).
[17]D. C. Abbas, T. J. Aton, and C. P. Slichter, Phys. Rev. Lett. 41, 719 (1978); see also, D. C. Abbas, Ph.D. thesis (University of Illinois, 1977) (unpublished).
[18]F. Herman and S. Skillman, *Atomic Structure Calculations* (Prentice-Hall, Englewood Cliffs, 1963).
[19]For a discussion of the rationale behind selection of a similar potential, see, M. A. Ball, J. R. Asik, and C. P. Slichter, Phys. Rev. 181, 662 (1969).
[20]C. M. Hurd, J. Phys. Chem. Solids 30, 539 (1968).
[21]Making a reasonable estimate for the amount of *s*- and *p*-wave scattering changes this value by only about 5%, to 2.05 $\mu\Omega$ cm/at. %.
[22]F. Richter and W. Kierspe, Z. Naturforsch. Teil A 20, 1371 (1965).
[23]R. E. Walstedt and L. R. Walker, Phys. Rev. B 11, 3280 (1975).
[24]R. E. Walstedt and Y. Yafet, Solid State Commun. 15, 1855 (1974).
[25]J. L. Tholence and R. Tournier, Phys. Rev. Lett. 25, 867 (1970).
[26]H. Alloul, J. Darville, and P. Bernier, J. Phys. F 4, 2050 (1974).
[27]P. Monod and S. Schultz, Phys. Rev. 173, 645 (1968).
[28]M. Vochten, M. Labro, and S. Vynckier, Physica (Utrecht) 86–88B, 467 (1977).
[29]L. L. Hirst, Z. Phys. 241, 9 (1971).
[30]L. L. Hirst, Adv. Phys. 21, 759 (1972).
[31]D. M. Follstaedt, D. Abbas, T. S. Stakelon, and C. P. Slichter, Phys. Rev. B 14, 47 (1976).
[32]D. C. Lo, D. V. Lang, J. B. Boyce, and C. P. Slichter, Phys. Rev. B 7, 973 (1973).
[33]W. Kohn and S. H. Vosko, Phys. Rev. 119, 912 (1960).
[34]This table corrects an error presented in an earlier account of our results (Ref. 13) due to incorrectly computing the normalization factor in Eq. (B3). This correction uniformly increases the calculated values of the anisotropic Knight-shift components by 26%.
[35]H. Alloul and H. Ishii, J. Phys. Lett. 38, 449 (1977).
[36]Paul L. Sagalyn and Michael N. Alexander, Phys. Rev. B 15, 5581 (1977).
[37]W. B. Pearson, *Lattice Spacings and Structures of Metals and Alloys* (Pergamon, New York, 1958).
[38]A. J. Heeger, A. P. Klein, and P. Tu, Phys. Rev. Lett. 17, 803 (1966).
[39]R. E. Walstedt and L. R. Walker, Phys. Rev. B 9, 4857 (1974).
[40]D. Pines, in *Solid State Physics*, edited by F. Seitz and D. Turnbull (Academic, New York, 1955), Vol. 1, p. 367.
[41]Rudi Hendel, Ph.D. thesis (University of Oregon, 1979) (unpublished).
[42]B. Cogblin and A. Blandin, Adv. Phys. 17, 281 (1968).
[43]S. E. Barnes, J. Phys. F 6, 115 (1976).
[44]S. E. Barnes, J. Phys. F 6, 1375 (1976).
[45]P. S. Bagus, T. L. Gilbert, and C. C. J. Roothan, J. Chem. Phys. 56, 5195 (1972).